# Electronic transitions of cobalt carbide, CoC, near 750 nm: A good example of case ($b_{\beta S}$) hyperfine coupling

M. Barnes, A. J. Merer, and G. F. Metha
*Department of Chemistry, University of British Columbia, Vancouver, British Columbia V6T 1Z1, Canada*

(Received 12 July 1995; accepted 14 August 1995)

The laser induced fluorescence spectrum of jet-cooled CoC near 750 nm has been measured at high resolution following the reaction of laser-ablated cobalt atoms with methane. The $X^2\Sigma^+$ ground state of CoC is an unusually good example of Hund's case ($b_{\beta S}$) coupling. Since Co has a nuclear spin $I=7/2$, each rotational level is split by the Fermi contact interaction into $G=3$ and $G=4$ components, where **G=I+S**; the splitting for $N=0$ is more than 0.5 $cm^{-1}$. The $X^2\Sigma^+$ state begins to uncouple toward case ($b_{\beta J}$) with increasing rotation. Transitions to various $^2\Pi$ excited states occur in the region 13 000–14 500 $cm^{-1}$; the most prominent of these (for which high resolution spectra have been recorded) lie at 13 079 $cm^{-1}$ ($^2\Pi_{3/2}$) and 13 343 $cm^{-1}$ ($^2\Pi_{1/2}$). The ($b_{\beta S}$) coupling in the ground state produces some unexpected hyperfine intensity patterns, which have been studied in detail. A very low-lying $^2\Delta_i$ state, whose $\Omega=5/2$ and $\Omega=3/2$ components lie at 221 and 1173 $cm^{-1}$, has been identified. Laser excitation of the $^2\Pi_{3/2}$–$^2\Delta_{5/2}$ transition has been observed by monitoring the strong $^2\Pi_{3/2}$–$X^2\Sigma^+$ emission, which has allowed the $^2\Delta_{5/2}$ state to be characterized at high resolution. A total of 879 rotational-hyperfine transitions between the various $^2\Pi_{1/2}$, $^2\Pi_{3/2}$, $^2\Delta_{5/2}$, and $^2\Sigma^+$ states have been assigned and fitted. Matrix elements for a $^2\Sigma^+$ state in case ($b_{\beta S}$) coupling are listed. © *1995 American Institute of Physics.*

## I. INTRODUCTION

Diatomic metal carbides have not received the same attention from high resolution spectroscopists as the corresponding oxides and nitrides. For many years the rotational analyses of the electronic spectra of PtC,[1–3] RhC,[4–6] IrC,[7,8] and RuC (Refs. 9 and 10) by Scullman and co-workers at Stockholm gave the only structural data available for diatomic metal carbides. Last year an analysis of the YC spectrum was published by Simard *et al.*;[11] PtC has recently been re-examined at high resolution by Steimle *et al.*[12] and the discovery and analysis of band systems of the FeC molecule has just been reported by Balfour *et al.*[13] FeC is the only 3*d* carbide for which rotational data are available, although band systems of VC and TiC have been recorded at low resolution using resonance enhanced multiphoton ionization.[14] Electron spin resonance spectra of RhC,[15] VC,[16,17] and NbC (Ref. 17) have been reported by Weltner and co-workers; the latter two are interesting as being examples of where the orbital angular momentum of the ground state is quenched in the matrix environment.

In this paper we report rotational and hyperfine analyses of electronic band systems of CoC at wavelengths around 750 nm. The CoC molecule is isoelectronic with MnO of which all the states analyzed so far are $^6\Sigma^+$.[18–20] By contrast CoC has a $^2\Sigma^+$ ground state, with a very large Fermi contact interaction parameter; this produces an unusually good example of case ($b_{\beta S}$) hyperfine coupling, where the rotational lines are split into doublets whose separation for low $N$ is more than 0.5 $cm^{-1}$. The upper states of the 750 nm bands appear to be $^2\Pi$ states. A low-lying $^2\Delta$ state, whose $\Omega=5/2$ component lies only 221 $cm^{-1}$ above the ground state, also gives transitions to these $^2\Pi$ excited levels. These transitions represent the first gas phase spectra reported for CoC; a matrix e.s.r. spectrum previously attributed to CoC has recently been reassigned to the distorted $Co(CO)_4$ radical.[21]

Coincidentally, at the same time as our discovery of the 750 nm system, a second electronic system of CoC was found quite independently by Adam *et al.*;[22] this other system has a $^2\Sigma^+$ upper state, and its (0,0) band is now known to lie at 716 nm.

## II. EXPERIMENTAL DETAILS

CoC molecules were prepared by the reaction of laser-ablated cobalt atoms with methane under supersonic jet-cooled conditions, and their spectra have been recorded by laser-induced fluorescence; the apparatus used was patterned after that of Simard *et al.*[23]

Briefly, the output of a Nd:YAG laser operating at a power of about 1 mJ/pulse on its second harmonic ($\lambda=532$ nm) was focused with a 50 cm focal length lens onto the surface of a slowly rotating cobalt rod. The ablated metal reacted with a pulse of helium containing about 5% methane, originally at a backing pressure of 6 atm. The gaseous products were passed through a 1 cm long condensation tube into the main chamber of the apparatus, where the average pressure was about $2\times10^{-4}$ Torr. A tunable laser beam crossed the molecular beam 5 cm downstream from the point of ablation, exciting fluorescence; this was passed through a Spex 0.75 m monochromator, which eliminated emissions from unwanted impurity species, and was finally recorded by a cooled photomultiplier tube.

Two tunable laser systems have been used. For survey work a Lumonics Inc. model HD500 tunable dye laser pumped by a second Nd:YAG laser gave linewidths of about 0.06 $cm^{-1}$, while for high resolution work a Ti:sapphire laser (Coherent Inc. model 899-21) pumped by an $Ar^+$ laser gave experimental linewidths of about 100 MHz, limited by residual Doppler broadening in the molecular beam. Calibra-

 0021-9606/95/103(19)/8360/12/$6.00 

tion was provided for both the survey and the high resolution spectra by optogalvanic signals from a uranium–argon hollow cathode lamp, for which the line frequencies have been given by Palmer *et al.*[24] To interpolate between the uranium lines in the high resolution spectra, a portion of the tunable laser beam was sent to a temperature and pressure stabilized Fabry–Perot étalon, servo-locked to a stabilized helium–neon laser. The resulting markers, spaced by 750 MHz, can be identified uniquely by a Burleigh WA-20VIS wavemeter;[25] the various 1 $cm^{-1}$ scans of the tunable laser are then easily concatenated by a computer program, since the relative order numbers of the fringes are always known. The system is capable of relative calibration to an accuracy of about 10 MHz over several hundred $cm^{-1}$, though in the present spectra the relative accuracy of the line measurements is limited to about 15 MHz by the experimental widths of the lines and their signal-to-noise ratio.

Wavelength-resolved spectra have also been recorded by scanning the 0.75 m monochromator. Using a slit width of 1 mm, corresponding to a resolution of 11 Å, ground state frequencies could be determined to $\pm 5$ $cm^{-1}$.

The carrier of the spectra reported here is assigned unambiguously as CoC from the rotational constant, the half-integer angular momentum $J$, and the hyperfine structure. The hyperfine patterns show that an atom with $I=7/2$ is present, which is consistent with $^{59}$Co, and the rotational structure indicates that an atom with even atomic number from the second row of the Periodic Table is also present. Furthermore, the hyperfine patterns show that all rotational levels $N$ are present, thereby ruling out structures such as CCoC, which would have half the levels missing because of the zero spins of the equivalent C atoms. Spectra taken using $CD_4$ are identical to those taken using $CH_4$, showing that no hydrogen is present, while the $B''$ value of nearly 0.7 $cm^{-1}$ is too high for the carrier to be anything other than CoC.

## III. APPEARANCE OF THE SPECTRA

### A. Case ($b_{\beta S}$) hyperfine coupling in the $X^2\Sigma^+$ ground state

The two strongest bands in the near-infrared laser-induced fluorescence spectrum of CoC appear near 760 nm. Low resolution tracings of these bands, which lie at 13 079 and 13 343 $cm^{-1}$, are shown in Figs. 1 and 2. Analysis of spectra taken at high resolution shows that they are $^2\Pi$–$^2\Sigma$ subbands and that the prominent line doubling of about 0.5 $cm^{-1}$ arises because the common $^2\Sigma^+$ lower state is in case ($b_{\beta S}$) hyperfine coupling.[26]

The conditions for this type of coupling to occur have been discussed by Dunn.[27] In a pure Hund's case (b) $^2\Sigma$ state, the electron spin **S** is not coupled to any other vector and precesses freely; in practice there will always be a small spin–rotation interaction, described by the operator $\gamma \mathbf{N}\cdot\mathbf{S}$. If a nucleus with nonzero spin **I** is also present there will be magnetic hyperfine interaction between the nuclear and electron spins. The resulting energy level pattern depends on which of these two interactions is the larger. The usual situation is that the hyperfine interaction is small compared to the spin–rotation coupling, which means that the logical

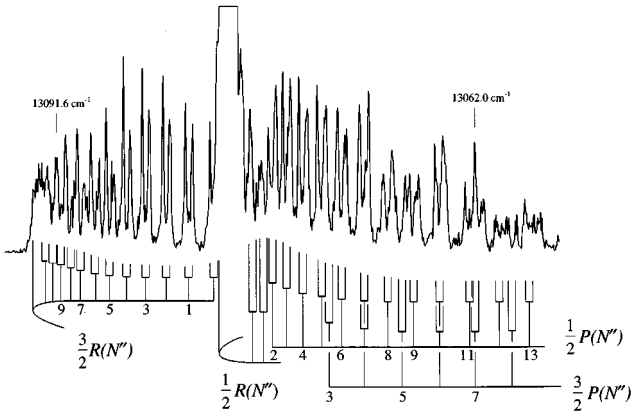


FIG. 1. Pulsed laser (survey) spectrum of the $^2\Pi_{3/2}$–$^2\Sigma^+$ subband of CoC at 13 079 $cm^{-1}$ showing the characteristic $G$-doubling caused by the case ($b_{\beta S}$) spin coupling in the ground state.

choice of basis set is given by the coupling scheme

$$\mathbf{N}+\mathbf{S}=\mathbf{J}; \quad \mathbf{J}+\mathbf{I}=\mathbf{F}, \tag{1}$$

which is called case ($b_{\beta J}$). It can happen that the Fermi contact hyperfine interaction is particularly large if the unpaired electron is in a molecular orbital which is almost unchanged from an $s$ atomic orbital; in this situation the Fermi contact operator, $b_F$ $\mathbf{I}\cdot\mathbf{S}$, couples the vector **S** to **I** more strongly than the spin–rotation interaction couples it to **N**. The logical choice of basis is then

$$\mathbf{S}+\mathbf{I}=\mathbf{G}; \quad \mathbf{N}+\mathbf{G}=\mathbf{F}, \tag{2}$$

which is called case ($b_{\beta S}$). The intermediate quantum number $G$ is that for the total spin, electron plus nuclear.[26,27] In a $^2\Sigma^+$ state there are two possible values of $G$, given by $I\pm 1/2$, so that each rotational level splits into two $G$-components.

The ground state of CoC is of this type; $^{59}$Co (the only stable isotope) has a spin $I=7/2$, which means that all the rotational levels are split into $G=3$ and 4 components, separated by roughly four times the Fermi contact parameter $b_F$. The Fermi contact parameter is particularly large in CoC,

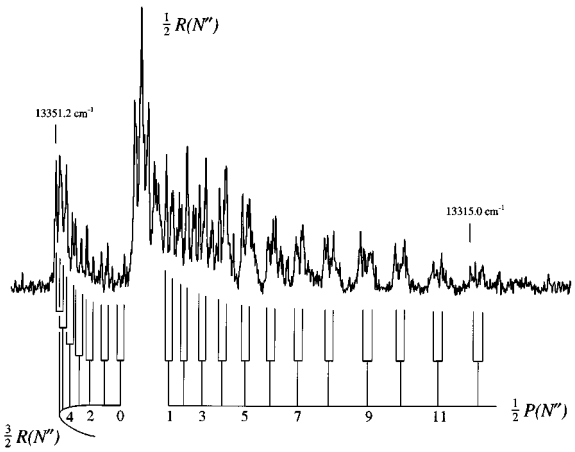


FIG. 2. Pulsed laser (survey) spectrum of the $^2\Pi_{1/2}$–$^2\Sigma^+$ subband of CoC at 13 343 $cm^{-1}$.

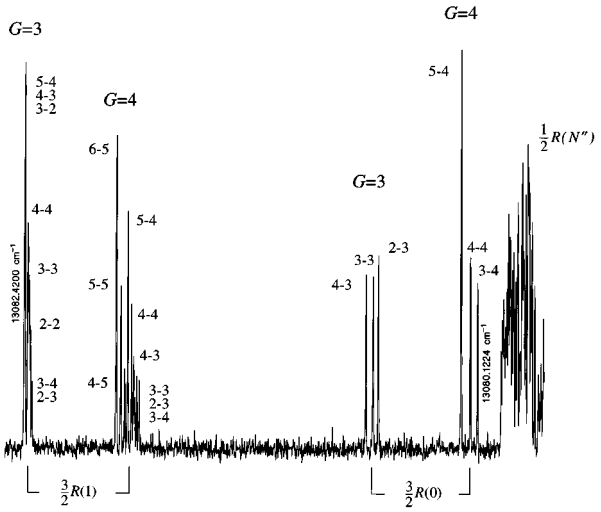


FIG. 3. High resolution spectrum of the $N=0$ and $N=1$ lines of the $3/2R$ branch of the $^2\Pi_{3/2}$–$^2\Sigma^+$ subband of CoC at 13 079 $cm^{-1}$ showing the individual hyperfine components.

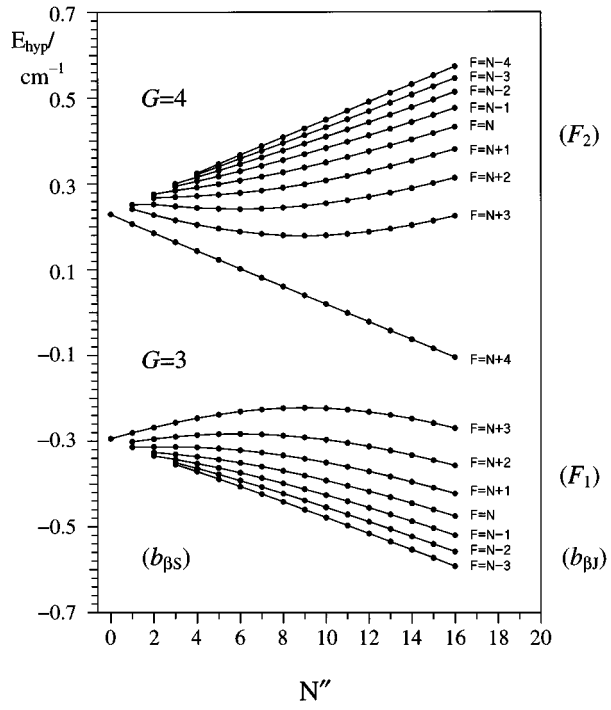


FIG. 4. Hyperfine energy levels of the $X\ ^2\Sigma^+$, $v=0$ level of CoC plotted against the rotational quantum number $N$ showing the uncoupling from case $(b_{\beta S})$ toward case $(b_{\beta J})$. Levels are calculated from the final least squares constants of Table II. The nuclear spin of $^{59}$Co is $I=7/2$.

and the observed splitting between the two components is more than 0.5 $cm^{-1}$. The only known case $(b_{\beta S})$-coupled $^2\Sigma^+$ state where the $G$-splitting is larger is the ground state of LuO, though the individual hyperfine components have not been resolved in its spectrum.[28,29]

Subbands of a similar form to the CoC bands shown in Figs. 1 and 2 were encountered in the ScO spectrum,[30] where the nuclear spin of $^{45}$Sc is also 7/2. Their structures differ slightly from $^2\Pi$–$^2\Sigma$ subbands as normally encountered because of the characteristic $G$-doubling which is independent of $N$. If there is no spin-splitting in the $^2\Sigma$ state a $^2\Pi$–$^2\Sigma$ subband has four branches, with $(J'-N'')=\pm 3/2$ and $\pm 1/2$, as has been described in detail by Herzberg.[31] A convenient, though seldom used, branch notation was proposed by Mulliken[32] who labeled them $3/2R$, $1/2R$, $1/2P$, and $3/2P$. Spin–rotation interaction in the $^2\Sigma$ state splits both the $1/2R$ and the $1/2P$ branches into two, giving six branches altogether; the outer two branches, $3/2R$ and $3/2P$, are not split because the $\Delta J=0,\pm 1$ selection rule is only satisfied by one of the two lower state spin components, namely, that with $|J'-J''|=1$. When the $^2\Sigma$ state is in case $(b_{\beta S})$ coupling all four branches, $3/2R$, $1/2R$, $1/2P$, and $3/2P$, show the $G$-doubling of the $N''$ lower level, giving a total of eight branches.

Figure 3 shows the first lines of the $3/2R$ branch of the 13 079 $cm^{-1}$ subband. This branch corresponds to the $R_1$ branch of a $^2\Pi_i$–$^2\Sigma^+$ transition, and would not be expected to show the spin-doubling of the $^2\Sigma^+$ state. The fact that the $N=0$ line is split into two groups of hyperfine components is clear proof of the case $(b_{\beta S})$ coupling. The energy level pattern for the ground state is given in Fig. 4. The contribution of the spin–rotation coupling to the energy increases with the rotational quantum number $N$, so that with increasing rotation the spin coupling changes progressively over to case $(b_{\beta J})$. In the CoC spectrum we see the uncoupling process beginning, but it is by no means complete even at the highest $N$ values observed.

The upper states of the 13 079 and 13 343 $cm^{-1}$ bands are shown by the rotational analysis to have $\Omega'=3/2$ and 1/2, respectively, and with the strong $Q$ branches suggesting a $\Delta\Lambda=1$ transition, it would seem logical to assign them as the spin–orbit components of a $^2\Pi$ state. However, the degradation of the two subbands is very different; the rotational constants for the two upper levels are $B'=0.626$ and 0.571 $cm^{-1}$, respectively.

### B. A very low-lying $^2\Delta$ state

The wavelength-resolved fluorescence patterns from the subbands at 13 079 and 13 343 $cm^{-1}$ are shown in Fig. 5. The $^2\Pi_{3/2}$ subband at 13 079 $cm^{-1}$ gives a clear ground state vibrational progression with intervals $\Delta G_{1/2}=934$ $cm^{-1}$ and $\Delta G_{3/2}=913$ $cm^{-1}$. (The notation $\Delta G_{v+1/2}$ used here is the standard notation for vibrational intervals,[31] and $G$ should not be confused with the angular momentum quantum number of Sec. III A.) In addition two other levels appear, at 221 and 1059 $cm^{-1}$ above the ground state. The $^2\Pi_{1/2}$ subband at 13 343 $cm^{-1}$ gives an identical ground state progression, but the additional levels are shifted up by 952 $cm^{-1}$ to 1173 and 2011 $cm^{-1}$. Since the $\Omega'$ values of the two substates are different, it is logical to assign the additional features as going to the two spin components of a low-lying orbitally degenerate electronic state, where the spin–orbit splitting is slightly larger than the vibrational frequency.

By tuning the laser in the region around 12 850 $cm^{-1}$, we were able pump the $^2\Pi_{3/2}$ state from the new level at 221 $cm^{-1}$; by monitoring the fluorescence at 13 079 $cm^{-1}$ back to the $^2\Sigma^+$ ground state, we obtained the spectrum shown in

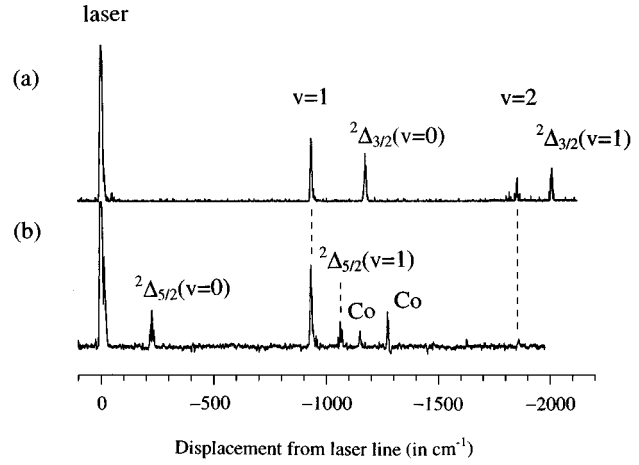


FIG. 5. Wavelength-resolved fluorescence from (a) the $^2\Pi_{1/2}$ state of CoC at 13 343 cm$^{-1}$ and (b) the $^2\Pi_{3/2}$ state of CoC at 13 079 cm$^{-1}$. These spectra show the vibrational structure of the $X\ ^2\Sigma^+$ state and features arising from the low-lying $A\ ^2\Delta_i$ state.

Fig. 6. This is a remarkable band, completely undegraded and looking more like an infrared vibrational fundamental than an electronic transition. Even at this resolution it is clear that the $P$ branch is stronger than the $R$ branch and that the first $R$ and $P$ lines have $J''=5/2$; the transition is therefore $^2\Pi_{3/2}$–$^2\Delta_{5/2}$. It has been possible to record the band at high resolution, and to obtain a detailed analysis of the hyperfine structure. Unfortunately it was not possible to do the same for the state at 1173 cm$^{-1}$, but there seems to be little doubt that it represents the $^2\Delta_{3/2}$ component, and that the spin–orbit splitting constant $A$ is $-476$ cm$^{-1}$. This new $^2\Delta$ state will be designated the $A\ ^2\Delta_i$ state.

It is perhaps not surprising that we can excite transitions out of the $^2\Delta_{5/2}$ level at 221 cm$^{-1}$. Low-lying metastable excited states up to 3000 cm$^{-1}$ above the ground level are found to be populated in $Nb_2$ (Ref. 32) and MnF (Ref. 33) in experiments using a similar ablation source. From our high resolution spectra it is estimated that the $^2\Pi_{3/2}$–$^2\Delta_{5/2}$ (0,0) band is only a factor of 2 weaker than the $^2\Pi_{3/2}$–$X\ ^2\Sigma^+$ (0,0) band.

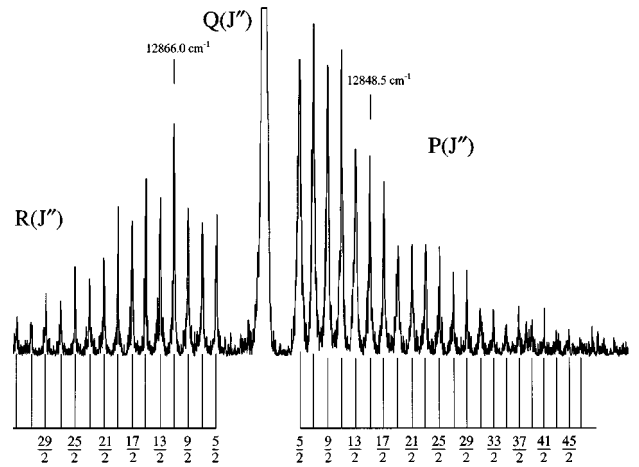


FIG. 6. Survey spectrum of the $^2\Pi_{3/2}$–$^2\Delta_{5/2}$ subband of CoC near 12 858 cm$^{-1}$. This spectrum was recorded by monitoring the $^2\Pi_{3/2}$–$^2\Sigma^+$ fluorescence at 13 079 cm$^{-1}$.

### C. $^2\Pi$ upper states near 14 000 cm$^{-1}$

Lying just to the short wavelength side of the 760 nm bands are four more bands, also of $^2\Pi$–$^2\Sigma^+$ type, which have proved to be too weak for high resolution rotational and hyperfine analysis. It has been possible to establish their $\Omega'$ values from the patterns of wavelength resolved fluorescence that they give, since each $^2\Pi$ upper level also fluoresces to the $A\ ^2\Delta$ state, but only to one spin component of it according to the selection rule $\Delta\Sigma=0$. At 13 428 cm$^{-1}$, close to the $^2\Pi_{1/2}$–$X\ ^2\Sigma^+$ subband of Fig. 2, is a band which, on excitation, gives emission to the $A\ ^2\Delta_{5/2}$ component and therefore has $\Omega'=3/2$. It has been possible to estimate the upper state $B$ value from the separation of the two heads formed by the $3/2R$ and $1/2R$ branches to obtain $B'\sim 0.55_3$ cm$^{-1}$. This band is illustrated in Fig. 7(a).

About 1000 cm$^{-1}$ further to the blue are three more weak bands. The upper level of the band at 14 071 cm$^{-1}$, shown in Fig. 7(b), emits only to the $A\ ^2\Delta_{5/2}$ component and presumably has $\Omega'=3/2$. A partial rotational analysis has been possible from the low resolution spectra; the upper state constants are $B'=0.5551(16)$ cm$^{-1}$ and $D'=-4.40(14)\times 10^{-5}$ cm$^{-1}$. Another band, near 14 140 cm$^{-1}$ [Fig. 7(c)], is completely unresolved at low resolution but the upper level is also assigned as having $\Omega'=3/2$ since it emits to the $A^2\Delta_{5/2}$ component. This upper state is provisionally assigned as $^2\Pi_{3/2}$, $v=1$. The highest energy subband we have found involves an $\Omega'=1/2$ upper level at 14 470 cm$^{-1}$ [Fig. 7(d)]; the separation of $R$ and $Q$ heads gives the rotational constant $B'\sim 0.60_5$ cm$^{-1}$. This upper state is assigned as $^2\Pi_{1/2}$, $v=1$.

The only other transitions we have observed in this region are the (0,0) and (1,0) bands of the $^2\Sigma^+$–$X\ ^2\Sigma^+$ system currently under investigation by Adam *et al.*[22] These bands lie at 13 950 (716 nm) and 14 635 cm$^{-1}$ (683 nm), respectively, and both have $B'\sim 0.52$ cm$^{-1}$.

## IV. ROTATIONAL AND HYPERFINE HAMILTONIAN

The full rotational and hyperfine Hamiltonian for the $^2\Sigma^+$ ground state is given by

$$H=B\mathbf{N}^2-D\mathbf{N}^4+\gamma\mathbf{N}\cdot\mathbf{S}+b\mathbf{I}\cdot\mathbf{S}+cI_zS_z + eT^2(\mathbf{Q})\cdot T^2(\nabla E). \quad (3)$$

The terms are identified by the parameters appearing; $B$ and $D$ are the rotational constant and its centrifugal distortion, $\gamma$ is the spin–rotation parameter, $b$ is the contact parameter, and $c$ is the dipolar interaction, while the last term is the nuclear electric quadrupole coupling. The magnetic hyperfine terms have been taken according to Frosch and Foley's definition,[35] where the true Fermi contact parameter $b_F$ is equal to $b+c/3$. The only field gradient constant needed for a $\Sigma$ state is defined by

$$eq_0=2\langle\eta,\Lambda=0|T_0^2(\nabla E)|\eta,\Lambda=0\rangle. \quad (4)$$

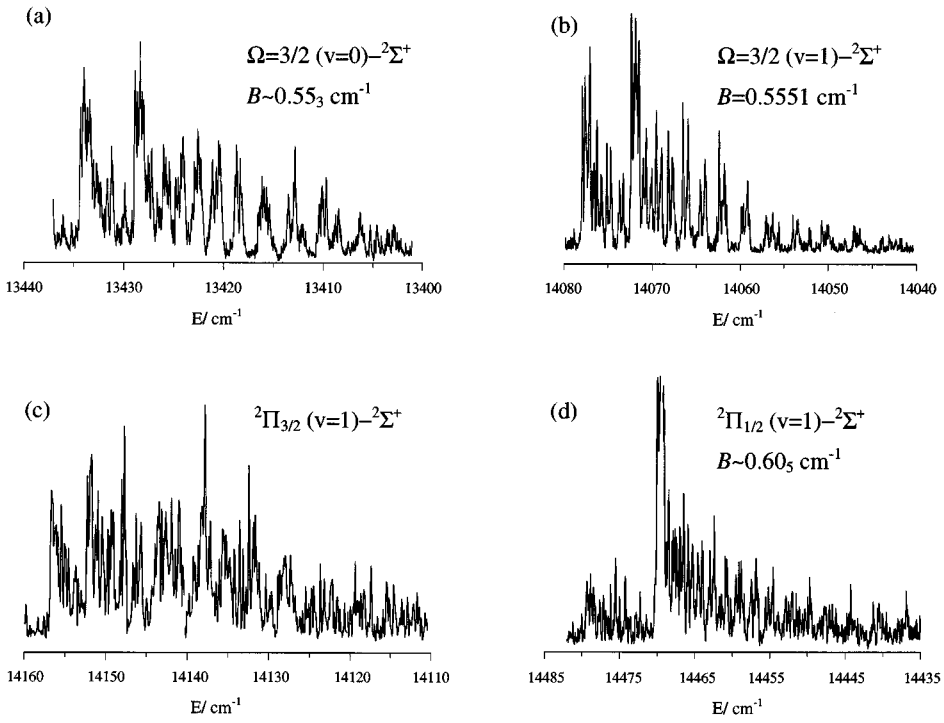


FIG. 7. Low resolution spectra of four weak subbands of CoC in the 14 000 cm$^{-1}$ region.

We have chosen to work in the case ($b_{\beta S}$) basis of Eq. (2) in order to avoid possible eigenvalue sorting problems in the matrix diagonalization. The rotational energy is obviously $BN(N+1)-DN^2(N+1)^2$, while from the definition $\mathbf{S}+\mathbf{I}=\mathbf{G}$ the contact term has only the diagonal elements

$$\langle N(SI)GF|b\mathbf{I}\cdot\mathbf{S}|N(SI)GF\rangle = \frac{b}{2}[G(G+1)-I(I+1)-S(S+1)]. \tag{5}$$

The matrix elements of Eq. (5) are responsible for nearly all of the 0.5 cm$^{-1}$ splitting between the $G=3$ and 4 spin levels; for $G=3$ and 4 the contact energies are $-9b/4$ and $7b/4$, respectively. The spin–rotation interaction is described by the tensor expression

$$\begin{aligned}\langle N'(SI)G'F|\gamma\mathbf{N}\cdot\mathbf{S}|N(SI)GF\rangle &= \gamma(-1)^{N+G'+F}\begin{Bmatrix} F & G' & N \\ 1 & N & G\end{Bmatrix}\sqrt{N(N+1)(2N+1)} \\ &\times(-1)^{I+S+G+1}\sqrt{(2G+1)(2G'+1)} \\ &\times\begin{Bmatrix} I & G' & S \\ 1 & S & G\end{Bmatrix}\sqrt{S(S+1)(2S+1)}.\end{aligned} \tag{6}$$

Its diagonal element reduces to

$$\langle N,G,F|\gamma\mathbf{N}\cdot\mathbf{S}|N,G,F\rangle = -\gamma\frac{[F(F+1)-G(G+1)-N(N+1)][I(I+1)-G(G+1)-S(S+1)]}{4G(G+1)}, \tag{7}$$

or specifically,[30]

$$-\frac{\gamma}{16}[F(F+1)-N(N+1)-12]$$

for $G=3$ and

$$\frac{\gamma}{16}[F(F+1)-N(N+1)-20]$$

for $G=4$. The off-diagonal element is

$$\langle N,G-1,F|\gamma\mathbf{N}\cdot\mathbf{S}|N,G,F\rangle = \gamma\frac{[Y(FNG)Y(ISG)]}{4G\sqrt{(2G+1)(2G-1)}}, \tag{8}$$

where

$$Y(abc)=\sqrt{(a+b+c+1)(b+c-a)(a+c-b)(a+b-c+1)}. \tag{9}$$

The matrix elements of Frosch and Foley's dipolar term,[35] $cI_zS_z$, can be calculated from those of the full dipolar Hamiltonian,

$$H_{\text{dipolar}}=-g\mu_B g_N\mu_N r^{-3}\sqrt{10}T^1(\mathbf{I})\cdot T^1(\mathbf{S},C^2), \tag{10}$$

which are

$$\langle N'\Lambda'(SI)G'F|H_{\text{dipolar}}|N\Lambda(SI)GF\rangle$$
$$=\sqrt{30}g\mu_B g_N\mu_N(-1)^{N+G'+F}\begin{Bmatrix}F & G' & N'\\ 2 & N & G\end{Bmatrix}\sqrt{I(I+1)(2I+1)}\sqrt{S(S+1)(2S+1)}\sqrt{(2G+1)(2G'+1)}$$
$$\times\begin{Bmatrix}S & S & 1\\ I & I & 1\\ G' & G & 2\end{Bmatrix}\sum_q(-1)^{N'-\Lambda'}\sqrt{(2N+1)(2N'+1)}\begin{pmatrix}N & 2 & N\\ -\Lambda & q & \Lambda\end{pmatrix}\langle\Lambda'|T_q^2(C^2)r^{-3}|\Lambda\rangle. \tag{11}$$

The parameter $c$ is given by

$$c=3g\mu_B g_N\mu_N\langle\Lambda'|T_0^2(C^2)r^{-3}|\Lambda\rangle, \tag{12}$$

where the $q=0$ index implies the second rank spherical component $(c/3)(3I_zS_z-\mathbf{I}\cdot\mathbf{S})$, rather than $cI_zS_z$. It is easily shown, with the help of Eq. (5), that the matrix elements of $cI_zS_z$ are obtained by adding $-3c/4$ and $7c/12$, respectively, to the algebraic expressions for $G=3$ and 4 given by Eq. (11).

The tensor expression for the quadrupole Hamiltonian, as needed for $\Sigma$ electronic states, is

$$\langle N'(SI)G'F|eT^2(\mathbf{Q})\cdot T^2(\nabla E)|N(SI)GF\rangle=(-1)^{N+G'+F}\begin{Bmatrix}F & G' & N'\\ 2 & N & G\end{Bmatrix}\times(-1)^{I+S+G'}\sqrt{(2G+1)(2G'+1)}$$
$$\times\begin{Bmatrix}S & I & G\\ 2 & G' & I\end{Bmatrix}\frac{1}{4}e^2Qq_0\sqrt{\frac{(2I+1)(2I+2)(2I+3)}{2I(2I-1)}}$$
$$\times(-1)^{N'}\sqrt{(2N+1)(2N'+1)}\begin{pmatrix}N & 2 & N\\ 0 & 0 & 0\end{pmatrix}. \tag{13}$$

The matrix elements of the full $^2\Sigma^+$ Hamiltonian are shown in algebraic form in Table I.

Since the two excited states at 13 079 and 13 343 $\text{cm}^{-1}$ have such comparatively different $B'$ values we have not attempted to fit them together, but have taken them as two separate case $(c)$ states. In the same way we have treated the $A\,^2\Delta_{5/2}$ substate as an isolated case $(c)$ state. The Hamiltonian used was

$$H=B\mathbf{R}^2-D\mathbf{R}^4+H\mathbf{R}^6+H_{\text{LD}}+H_{\text{mag.hfs}}+H_{\text{quadrupole}}, \tag{14}$$

where the $\Lambda$-doubling is represented by

$$H_{\text{LD}}=\frac{1}{2}(p+2q)(J_+S_+e^{-2i\phi}+J_-S_-e^{2i\phi})$$
$$-\frac{1}{2}q(J_+^2e^{-2i\phi}+J_-^2e^{2i\phi}), \tag{15}$$

the magnetic hyperfine structure by the Hamiltonian

$$H_{\text{mag.hfs}}=aI_zI_z+b\mathbf{I}\cdot\mathbf{S}+cI_zS_z$$
$$+\frac{1}{2}d(I_-S_-e^{2i\phi}+I_+S_+e^{-2i\phi}), \tag{16}$$

and the quadrupole coupling is as before. The $\Lambda$-doubling terms in $p+2q$ and $d$ are needed for the $^2\Pi_{1/2}$ substate, while the $q$ term is needed for $^2\Pi_{3/2}$, where it is taken in the form $\mp q_{\text{eff}}(J-1/2)(J+1/2)(J+3/2)$ for the $e$ and $f$ levels, respectively. Centrifugal distortion of the $\Lambda$-doubling parameter $p+2q$ is also required; its matrix elements are obtained by matrix multiplication from the matrices of $\mathbf{R}^2$ and Eq. (15). There is only one determinable hyperfine parameter for a substate in case $(c)$; it is written $h_\Omega=a\Lambda+(b+c)\Sigma$.[36] Since the tensorial and algebraic expressions have been presented before,[37,38] they will not be given here.

A data set consisting of 879 assigned hyperfine lines from the $^2\Pi_{1/2}$–$^2\Sigma^+$, $^2\Pi_{3/2}$–$^2\Sigma^+$, and $^2\Pi_{3/2}$–$^2\Delta_{5/2}$ transitions was fitted simultaneously. In the initial stages only the low $N$ lines were included, but in the end the complete data set up to $N=14$ could be used. A total of 29 parameters were floated in the final fit, giving a rms error of 0.000 588 $\text{cm}^{-1}$. The final constants are listed in Table II. For the ground state, all six parameters are well determined. Only the $e^2Qq_0$ constants for the $^2\Pi_{1/2}$, $^2\Pi_{3/2}$, and $^2\Delta_{5/2}$ states were not well determined.

## V. HYPERFINE LINE STRENGTH CONSIDERATIONS

The $^2\Pi_{3/2}$–$^2\Delta_{5/2}$ subband near 12 850 $\text{cm}^{-1}$ shows the familiar hyperfine intensity patterns for case $(a_{\beta J})$ coupling

TABLE I. Matrix of the rotational and hyperfine Hamiltonian for a $^2\Sigma^+$ state in case ($b_{\beta S}$) coupling, where one spinning nucleus with $I=7/2$ is present.

| | $\lvert G=4,N\rangle$ | $\lvert G=3,N\rangle$ |
|---|---|---|
| $\langle G=4,N\rvert$ | $BN(N+1)-DN^2(N+1)^2+\frac{\gamma}{16}[F(F+1)-N(N+1)-20]$<br>$+\frac{7}{4}b+\frac{7}{12}c-\left(c+\frac{3e^2Qq_0}{14}\right)[F(F+1)-N(N+1)-20]$<br>$\frac{3[F(F+1)-N(N+1)-19]-80N(N+1)}{48(2N-1)(2N+3)}$ | $\frac{\left\{\frac{\gamma}{16}-\left(c-\frac{e^2Qq_0}{14}\right)\frac{[F(F+1)-N(N+1)-15]}{16(2N-1)(2N+3)}\right\}}{\sqrt{(F+N+5)(F+N-3)(N-F+4)(F-N+4)}}$ |
| $\langle G=3,N\rvert$ | Symmetric | $BN(N+1)-DN^2(N+1)^2-\frac{\gamma}{16}[F(F+1)-N(N+1)-12]$<br>$-\frac{9}{4}b-\frac{9}{12}c-\left(-c+\frac{5e^2Qq_0}{14}\right)\times[F(F+1)-N(N+1)-12]$<br>$\frac{3[F(F+1)-N(N+1)-11]-48N(N+1)}{48(2N-1)(2N+3)}$ |
| $\langle G=4,N-2\rvert$ | $\left(c+\frac{3e^2Qq_0}{14}\right)\sqrt{(F+N+4)(F+N+5)(N-F+3)(N-F+4)}$<br>$\frac{\sqrt{(F+N-5)(F+N-4)(F-N+5)(F-N+6)}}{32(2N-1)\sqrt{(2N+1)(2N-3)}}$ | $\left(-c+\frac{e^2Qq_0}{14}\right)\sqrt{(F+N+4)(N-F+3)(F+N-5)(F+N-4)}$<br>$\frac{\sqrt{(F+N-3)(F-N+4)(F-N+5)(F-N+6)}}{32(2N-1)\sqrt{(2N+1)(2N-3)}}$ |
| $\langle G=3,N-2\rvert$ | $\left(c-\frac{e^2Qq_0}{14}\right)\sqrt{(F+N+3)(F+N+4)(F+N+5)(N-F+2)}$<br>$\frac{\sqrt{(N-F+3)(N-F+4)(F+N-4)(F-N+5)}}{32(2N-1)\sqrt{(2N+1)(2N-3)}}$ | $\left(-c+\frac{5e^2Qq_0}{14}\right)\sqrt{(F+N+3)(F+N+4)(N-F+2)(N-F+3)}$<br>$\frac{\sqrt{(F+N-4)(F+N-3)(F-N+4)(F-N+5)}}{32(2N-1)\sqrt{(2N+1)(2N-3)}}$ |

in both states. The $P(5/2)$ line is illustrated in Fig. 8, where it is seen that the strongest hyperfine components are those with $\Delta F=\Delta J$, and the intensities are smoothly varying functions of $F$. By contrast the $^2\Pi_{3/2}$–$X\ ^2\Sigma^+$ ($b_{\beta S}$) subband at 13 079 cm$^{-1}$ has some surprising irregularities. Detailed calculations of the line strengths show that these are the expected patterns for transitions between states in ($a_{\beta J}$) and ($b_{\beta S}$) coupling; since transitions of this type have not previously been studied in detail at hyperfine resolution it is worthwhile documenting what happens.

Figure 9 shows the hyperfine structure of the two $G$-components of the $1/2P(2)$ line of the $^2\Pi_{3/2}$–$X\ ^2\Sigma^+$ subband at 13 079 cm$^{-1}$. The hyperfine lines in Fig. 9 have been labeled $r$, $q$, and $p$, for $\Delta F=+1$, 0, and $-1$, respectively. It can be seen that the intensities of the $r$ and $q$ lines for $G=3$ and those of the $p$ and $q$ lines for $G=4$ pass through minima, with the $r(F=2)$, $G=3$ and $p(F=5)$, $G=4$ lines being completely absent. These minima can be thought of as resulting from interference between the transition moments of

TABLE II. Rotational and hyperfine constants for the three analyzed electronic states of CoC. All values are in cm$^{-1}$ and quoted errors in brackets are three standard deviations.[a]

| | $^2\Sigma^+$ | $^2\Delta_{5/2}$ | $^2\Pi_{3/2}$ | $^2\Pi_{1/2}$ |
|---|---|---|---|---|
| $T_\Omega$ | 0 | 221.229 97(71) | 13 079.135 40(18) | 13 343.040 80(34) |
| $A\Lambda$ | | −952.0[b] | | |
| $B$ | 0.693 750 2(92) | 0.626 799(51) | 0.625 656(12) | 0.571 275(33) |
| $\gamma$ | −0.041 110(33) | | | |
| $10^7D$ | 1.526(50) | 1.77(95) | −6.80(14) | −31.87(72) |
| $10^7\ H$ | | | −4.71(48) | −22.0(44) |
| $10^3\ (p+2q)$ | | | | −17.116(68) |
| $10^6\ q_{\rm eff}$ | | | −1.24(10) | |
| $10^5\ D_{(p+2q)}$ | | | | −5.330(72) |
| $h_\Omega$ | | 0.040 48(19) | 0.023 28(12) | 0.027 52(31) |
| $b$ | 0.128 808(83) | | | |
| $c$ | 0.006 44(21) | | | |
| $d$ | | | | 0.003 03(12) |
| $10^4\ c_I$ | | | 0.461(60) | −0.57(10) |
| $e^2Qq_0$ | 0.010 2(12) | −0.002 6(40) | 0.003 3(14) | 0.002 2(18) |
| $r_0$/Å | 1.561 2 | 1.642 4 | 1.643 9 | 1.720 4 |

[a]Fit to 879 transitions with a rms error of 0.000 588 cm$^{-1}$.
[b]From wavelength resolved fluorescence experiment. See text for details.

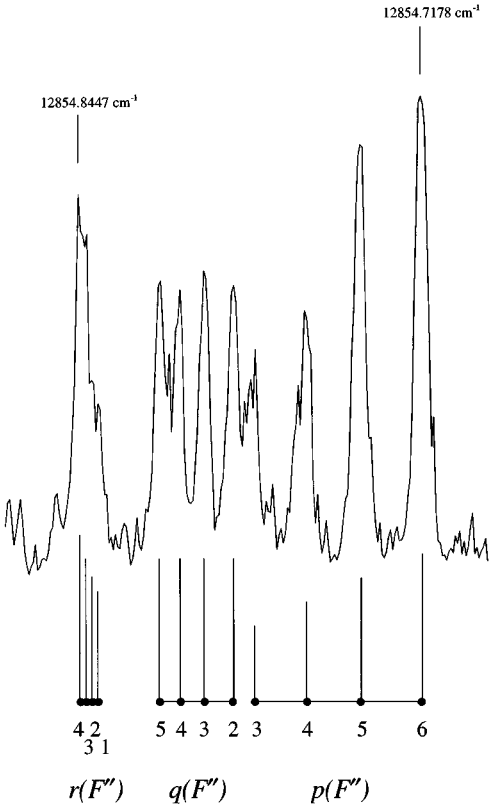


FIG. 8. Hyperfine structure of the $P(5/2)$ line of the $^2\Pi_{3/2}$–$^2\Delta_{5/2}$ subband of CoC near 12 858 $cm^{-1}$ (see Fig. 6).

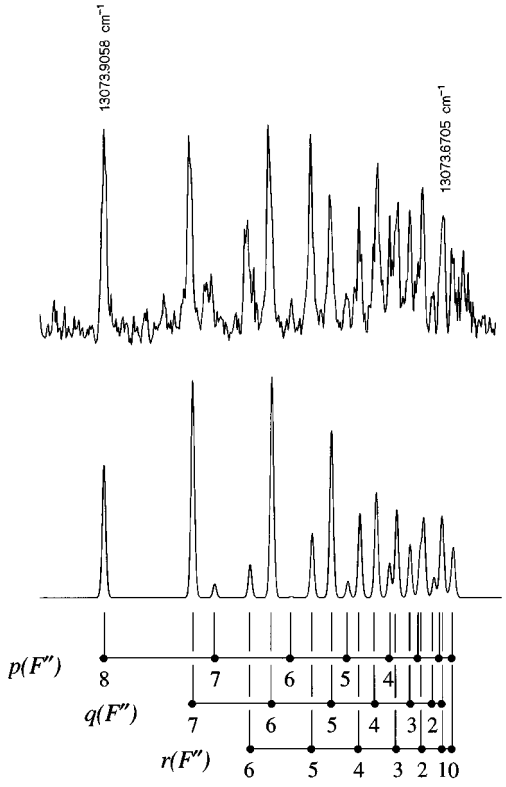


FIG. 10. Observed and calculated hyperfine structure of the $1/2P(4)$ line of the $^2\Pi_{3/2}$–$^2\Sigma^+$ subband of CoC near 13 079 $cm^{-1}$. Intermediate spin coupling is used for the ground state rotational-hyperfine wave functions.

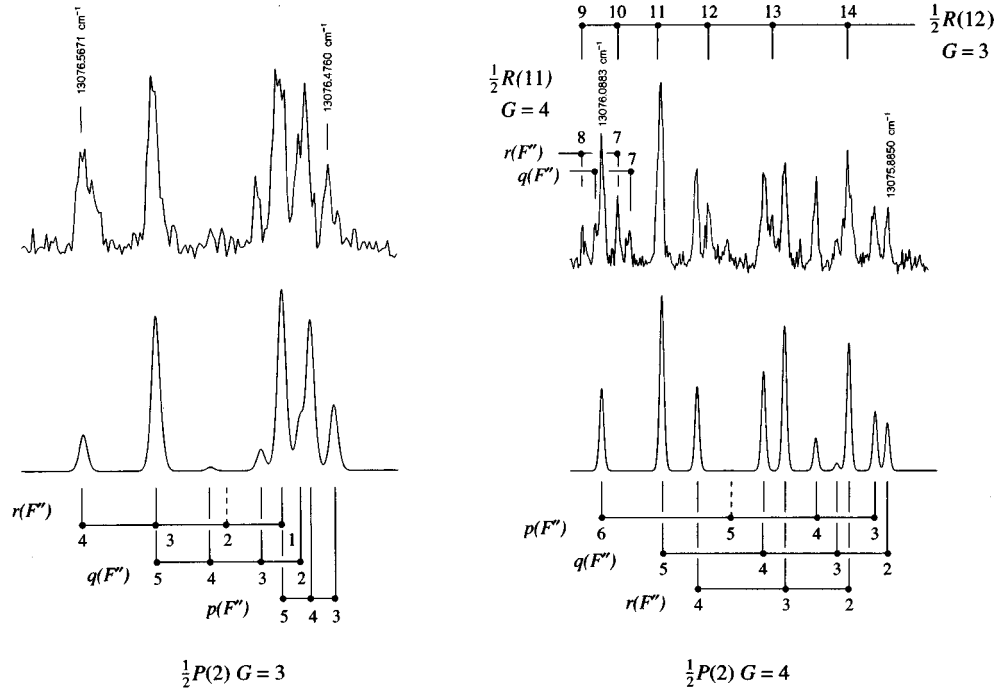


FIG. 9. Observed and calculated hyperfine structures of the $G=3$ and $G=4$ components of the $1/2P(2)$ line of the $^2\Pi_{3/2}$–$^2\Sigma^+$ subband of CoC near 13 079 $cm^{-1}$. Pure case ($b_{\beta S}$) coupling is assumed in the ground state.

what would be the ${}^{P}Q_{12}$ and $P_1$ branches in the absence of nuclear spin.

The line strengths for transitions where one of the states is in case $(b_{\beta S})$ coupling have been considered by Féménias *et al.*[39] and Brown *et al.*[37] The more complete treatment is that of Ref. 39, but unfortunately the formulas given there cannot be used directly with our energy matrices, since the derivation uses the ''méthode des Moments Inversés,'' where the choice of phases is not consistent with Sec. IV. We have rederived the expressions so as to be consistent and obtain the case $(a_{\beta J})-(b_{\beta S})$ line strength factors as

$$\begin{aligned}
&\langle \eta'\Lambda';S'\Sigma';J'\Omega'IF\|T^1(\mu)\|\eta\Lambda;N\Lambda(SI)GF\rangle \\
&\quad=\sum_J (-1)^{N+S+I+F}\sqrt{(2J+1)(2G+1)}\begin{Bmatrix} N & S & J \\ I & F & G\end{Bmatrix}(-1)^{J'+I+F+1}\sqrt{(2F+1)(2F'+1)}\begin{Bmatrix} J' & F' & I \\ F & J & 1\end{Bmatrix} \\
&\quad\times\sum_{\Sigma,\Omega}(-1)^{N-S+\Omega}\sqrt{2N+1}\begin{pmatrix} J & S & N \\ \Omega & -\Sigma & -\Lambda\end{pmatrix}\sum_q (-1)^{J'-\Omega'}\sqrt{(2J+1)(2J'+1)}\begin{pmatrix} J' & 1 & J \\ -\Omega' & q & \Omega\end{pmatrix} \\
&\quad\times\langle \eta'\Lambda';S'\Sigma'|T_q^1(\mu)|\eta\Lambda;S\Sigma\rangle\delta_{ss'}. \qquad (17)
\end{aligned}$$

In this equation the unprimed quantum numbers $J$, $\Omega$, and $\Sigma$ are dummy quantum numbers that occur because the case $(b_{\beta S})$ state has been expanded as a linear combination of case $(b_{\beta J})$ functions, which are themselves constructed from case $(a_{\beta J})$ functions; they are not useful for classifying the energy levels, but allow an interpretation in terms of more familiar quantities.

To calculate the line strengths for Fig. 9 numerically, the ${}^2\Pi$ state functions must be written as Wang combinations of signed quantum number basis functions, e.g.,

$$\begin{aligned}
|{}^2\Pi_{3/2},J',e\rangle=2^{-1/2}\left\{\left|\Lambda=1;\Sigma=\frac{1}{2},J',\Omega'=\frac{3}{2}\right\rangle\right. \\
\left.+\left|\Lambda=-1;\Sigma=-\frac{1}{2},J',\Omega'=\frac{3}{2}\right\rangle\right\}. \qquad (18)
\end{aligned}$$

This is no complication since there is only one electronic transition moment acting,

$$\begin{aligned}
\mu_\perp&=\left\langle \Lambda=1,\Sigma=\frac{1}{2}\middle| T_1^1(\mu)\middle|\Lambda=0^+,\Sigma=\frac{1}{2}\right\rangle \\
&=\left\langle \Lambda=-1,\Sigma=-\frac{1}{2}\middle| T_{-1}^1(\mu)\middle|\Lambda=0^+,\Sigma=-\frac{1}{2}\right\rangle, \qquad (19)
\end{aligned}$$

so that the two terms from Eq. (18) give the same result. Since $S=1/2$, the sum over the dummy variable $J$ in Eq. (17) consists of two terms, which correspond to the line strength factors for the ${}^{P}Q_{12}$ and $P_1$ branches of a transition where the hyperfine structure is negligible. In the present case the hyperfine line intensity is proportional to the square of the sum of contributions from the two rotational branches, where each is scaled by the 6-$j$ symbols of Eq. (17).

The way the scaling goes can be illustrated for the $G=4$ component. The product of the 6-$j$ symbols for the ${}^{P}Q_{12}$ branch has the same sign as that for the $P_1$ branch in the $r$-type hyperfine components, but opposite sign in the $p$-type components; since the sign of the 3-$j$ factors is the same for the two branches there can be no hyperfine intensity cancellation for the $r$-type components, but there happens to be an exact cancellation for the $p$-type components at $F'-F''=4-5$. For the $q$-type components, the ${}^{P}Q_{12}$ contribution passes through zero at $F'-F''=3-3$, in similar fashion to the intensity cancellations found in low-$JQ$ branches of case $(a_{\beta J})-(a_{\beta J})$ transitions[40] for large values of $I$; somewhere near this point the $q$-type hyperfine intensity, given by the square of the sum of the ${}^{P}Q_{12}$ and $P_1$ contributions, must therefore pass through zero. The weakest $q$-type line is in fact $F'-F''=3-3$, since the ${}^{P}Q_{12}$ rotational line strength factor is much greater than the $P_1$ factor.

Similar considerations hold for the $G=3$ component, with the difference that the 6-$j$ factors add for the $p$-type hyperfine components but subtract for the $r$-type; there is an exact cancellation for the $F'-F''=3-2$ component. In the $1/2P$ branches of a ${}^2\Pi_{1/2}$–$X\ {}^2\Sigma^+$ subband the signs of the rotational $P$ and $Q$ branch line strength factors are opposite, so that the $G=3$ hyperfine intensities behave roughly like the $G=4$ intensities of Fig. 9, and vice versa. The exact patterns are of course different because they reflect the second 3-$j$ symbol of Eq. (17), even though the 6-$j$ symbol factors are the same.

The calculated intensities shown in Fig. 9 assume pure case $(b_{\beta S})$ coupling in the $X\ {}^2\Sigma^+$ ground state. At this low $N$ value, $N=2$, the degree of uncoupling to case $(b_{\beta J})$ caused by the spin–rotation interaction is negligible. Figure 10 illustrates the $G=4$ component of a higher $N$ line, $1/2P(4)$, where this uncoupling is not negligible. The calculated intensities in Fig. 10 have been derived using exact intermediate coupling rotational-hyperfine wave functions, obtained from the eigenvectors of the $2\times2$ matrices given by the $G=3$ and 4 components for given $N$ and $F$. The main effect of the uncoupling is in the high $F$ lines, where it makes the intensity minimum in the $p$-type hyperfine components more pronounced, in better agreement with experiment. At higher $N$ values there is no minimum in the $q$-type line strength patterns, because the intensity cancellation effect of Ref. 40 only occurs when $J$ is less than $I$. The match between ex-

periment and calculation is not as good as in Fig. 9; it seems that saturation effects distort the experimental intensities of the strongest lines, as we found also in recent spectra of FeO taken with the same apparatus.[41]

## VI. DISCUSSION

### A. The $X\ ^2\Sigma^+$ state

A $^2\Sigma$ state in case ($b_{\beta S}$) coupling must always uncouple toward case ($b_{\beta J}$) with increasing rotation because of the spin–rotation interaction.[27] Figure 4 shows the hyperfine levels of the $X\ ^2\Sigma^+$ state of CoC plotted against $N$, using the final parameters from Table II. The uncoupling is comparatively rapid in CoC because of the large value of the spin–rotation parameter $\gamma$, and is well on its way to completion by $N=20$. The hyperfine energy order is opposite in the two spin-components, reflecting the difference in sign of the diagonal element of $\gamma\mathbf{N}\cdot\mathbf{S}$ for $G=3$ and 4. With increasing rotation, one of the nine hyperfine levels with $G=4$ must always move across to the $G=3$ group, where there are seven levels. This is because the two electron spin components in case ($b_{\beta J}$) coupling must have eight hyperfine levels each. When $b$ and $\gamma$ are of opposite sign, as in Fig. 4, the level that moves across is $F=N+4$; when $b$ and $\gamma$ have the same sign the level that moves is $F=N-4$.

It is no coincidence that the level patterns of Fig. 4 look exactly like that for the Zeeman splitting of a $^2$S atom with $I=7/2$ (see for example Fig. I.3 of Ref. 42). In both cases there is a scalar coupling of the electron spin **S** to a vector whose magnitude can be varied; in the Zeeman case it is the magnetic flux density **B** and in Fig. 4 it is the rotational angular momentum **N**. The only difference is that **B** is continuously tunable, whereas **N** corresponds to discrete rotational levels.

Turning to the hyperfine parameters, the experimental Fermi contact parameter, $b_F$, for the ground state is $b_F=b+c/3=0.130\ 95\ \mathrm{cm}^{-1}$. Given that the ground state comes from the electron configuration $(1\delta)^4(9\sigma)^1$, this value can be directly compared with the value of $b_F=0.147\ 12\ \mathrm{cm}^{-1}$ for the $4s$ orbital of the cobalt atom obtained from atomic beam studies.[43] The molecular value is 89% of the atomic value, indicating that the $9\sigma$ orbital is almost completely atomic $4s$ in character. Since the experimental $c$ parameter is small and positive, it is likely that the ground state contains a small contribution from an electron configuration that contains an unpaired $3d\sigma$ electron.

We can also predict a value of $b_F$ from the *ab initio* value of $\Psi^2_{4s}(0)$ (Ref. 44) using the expression

$$b_F=\frac{\mu_0}{4\pi hc}\times\frac{8\pi}{3}\times\frac{1}{2S}\times gg_N\mu_B\mu_N\langle\Psi^2(0)\rangle_{4s} \tag{20}$$

to calculate

$$b_F=0.003\ 186\ 25\times\frac{8\pi}{3}\times\frac{4.63}{7/2}\times 5.233$$
$$=0.1848\ \mathrm{cm}^{-1}.$$

This value is significantly larger than both the atomic and molecular $b_F$ values and indicates that the *ab initio* value of $\Psi^2_{4s}(0)$ is approximately 25% too large, as has generally been found for Hartree–Fock calculations.

### B. The $A\ ^2\Delta$ state

Apart from its rough position and vibrational frequency, we have no information about the $^2\Delta_{3/2}$ component of the $A\ ^2\Delta$ state. Therefore, although $h_{5/2}$ can be obtained from the $^2\Delta_{5/2}$ component there is insufficient information to obtain the hyperfine parameters separately. It seems clear that the $A\ ^2\Delta$ state arises from the electron configuration $(1\delta)^3(9\sigma)^2$, as we can verify by comparing with the Co atom. The hyperfine parameters for the $3d$ orbital of Co have been determined to be $a^{01}=0.0206$, $a^{10}=-0.007$, and $a^{12}=0.0286\ \mathrm{cm}^{-1}$, which are equivalent to $a$, $b_F$, and $c$. If the $3d\delta$ orbital is purely atomic in character, we can predict $h_{5/2}=0.0472\ \mathrm{cm}^{-1}$. The observed value, $h_{5/2}=0.040\ 48\ \mathrm{cm}^{-1}$, is 86% of the predicted value. This value can also be checked against *ab initio* calculations of the radial expectation value. Since only the unpaired $d\delta$ electron contributes, $b_F$ will be zero. We can calculate $a$ and $c$ from

$$a=\frac{\mu_0}{4\pi hc}\times gg_N\mu_B\mu_N\langle r^{-3}\rangle_{3d} \tag{21}$$

and

$$c=\frac{3}{2}\times\frac{\mu_0}{4\pi hc}\times\frac{1}{2S}\times gg_N\mu_B\mu_N$$
$$\times\langle 3\ \cos^2\ \theta-1\rangle_{d\delta}\langle r^{-3}\rangle_{3d}, \tag{22}$$

where $\langle 3\cos^2\theta-1\rangle_{d\delta}$ is the angular average.[45] These expressions give

$$a=0.003\ 186\ 25\times\frac{4.63}{7/2}\times 6.710=0.0283\ \mathrm{cm}^{-1}$$

and

$$c=\frac{3}{2}\times 0.003\ 186\ 25\times\frac{4.63}{7/2}\times\frac{-4}{7}\times 6.710$$
$$=-0.0243\ \mathrm{cm}^{-1},$$

resulting in an $h_{5/2}$ value of $0.0444\ \mathrm{cm}^{-1}$, in remarkably good agreement with the experimental value.

Since the $\delta^4\sigma^1\ X\ ^2\Sigma^+$ and $\delta^3\sigma^2\ A\ ^2\Delta_{3/2}$ states are almost degenerate, the energies of the two orbitals (in as much as orbitals exist) must be essentially equal. The spin–orbit parameter $A\Lambda\ (A\ ^2\Delta)=-952\ \mathrm{cm}^{-1}$ is very similar to those of the $Co^+$ ion and the diatomic molecules CoH and CoO. For comparison, $-2\zeta\ (3d)=-1072\ \mathrm{cm}^{-1}$ for the $Co^+$ ion,[46] $(4/3)A\Lambda=-971\ \mathrm{cm}^{-1}$ for the $X\ ^3\Phi$ ground state of CoH,[47] and $3A\Lambda=-997\ \mathrm{cm}^{-1}$ for the $X\ ^4\Delta$ ground state of CoO.[48] (The numerical factors here arise because of the different spin and orbital angular momentum quantum numbers of these different states.)

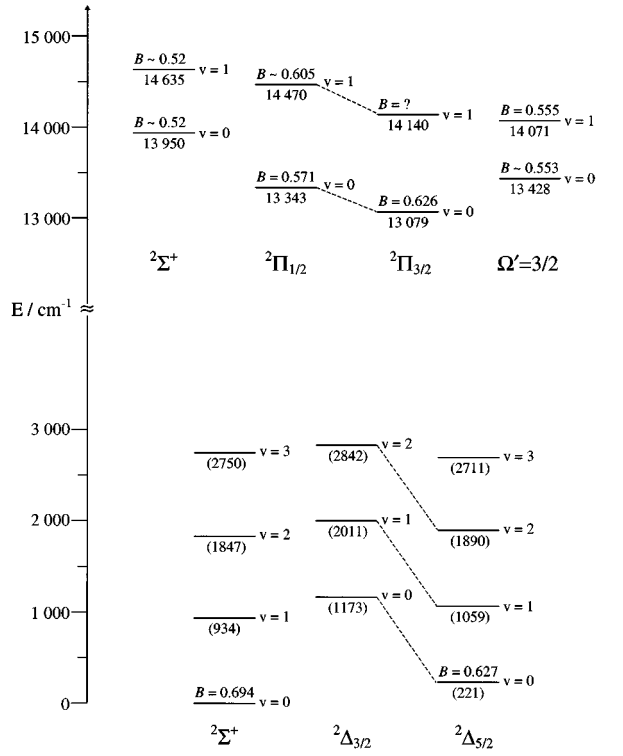


FIG. 11. Energy level diagram showing the vibrational levels of CoC observed in this work. The assignments to $^2\Pi$ and 3/2 levels are tentative (see text). The excited $^2\Sigma^+$ levels beginning at 13 950 cm$^{-1}$ belong to the system reported by Ref. 22.

### C. The $^2\Pi$ states

The various electronic and vibrational levels observed in this work are shown on the energy level diagram of Fig. 11. The intense bands at 13 079 and 13 343 cm$^{-1}$ and the weaker bands of Fig. 7 go to the groups of levels labeled $^2\Pi$ and $\Omega'=3/2$ in this diagram; in view of their irregular spacings and rotational constants the assignments given must be considered as provisional.

Three electron configurations give rise to low-lying $^2\Pi$ states, namely,

$$(3\pi)^3(1\delta)^4(9\sigma)^2 \quad ^2\Pi_i, \tag{A}$$

$$(3\pi)^4(1\delta)^4(4\pi)^1 \quad ^2\Pi_r, \tag{B}$$

$$(3\pi)^4(1\delta)^3(9\sigma)^1(4\pi)^1 \quad ^2\Pi_i(\text{also } ^4\Pi_i,\ ^2\Phi_i,\ ^4\Phi_i). \tag{C}$$

The evidence for choosing between them lies in the spin–orbit structure and the measured $h_\Omega$ parameters of the $^2\Pi_{1/2}$ level at 13 343 cm$^{-1}$ and the $^2\Pi_{3/2}$ level at 13 079 cm$^{-1}$. We find no further $^2\Pi$ levels below these two in our spectra, which suggests that they form the $v=0$ vibrational level of an *inverted* $^2\Pi$ state, though clearly heavily perturbed because their $B$ values differ by more than 0.05 cm$^{-1}$. This observation rules out configuration (B). Configuration (C), with its unpaired $4s\sigma$ electron ($9\sigma$), should have a large positive Fermi contact parameter, such that $h_{3/2}$ should be much larger than $h_{1/2}$. It is not possible to calculate its exact value because the configuration $\delta^3\sigma\pi$ gives two $^2\Pi$ states, whose electronic wave functions are mixtures of Slater determinants. Experimentally (see Table II), $h_{3/2}$ is less than $h_{1/2}$, which argues against configuration (C).

Configuration (A) is not ruled out, but attempts to reproduce the hyperfine $h$ parameters from the *ab initio* values of $\langle r^{-3}\rangle_{3d}$ and $\Psi^2_{4s}(0)$ are only partially successful. For example, the $3\pi$ orbital containing the unpaired electron is expected to be a mixture of carbon $2p\pi$ and cobalt $3d\pi$,

$$|3\pi\rangle = N|\text{Co},3d\pi\rangle + \sqrt{1-N^2}|\text{C},2p\pi\rangle, \tag{25}$$

where $N$ is a normalization coefficient; the cobalt hyperfine parameters are then estimated to be

$$\begin{aligned} a &= \frac{\mu_0}{4\pi hc}\times g g_N \mu_B \mu_N \langle r^{-3}\rangle_{3d} N^2 \\ &= 0.004\ 22\times\langle r^{-3}\rangle_{3d} N^2, \\ b_F &= 0, \\ c &= \frac{3}{2}\times\frac{\mu_0}{4\pi hc}\times g g_N \mu_B \mu_N \langle 3\ \cos^2\ \theta - 1\rangle_{d\pi}\langle r^{-3}\rangle_{3d} N^2 \\ &= 0.001\ 81\times\langle r^{-3}\rangle_{3d} N^2. \end{aligned} \tag{26}$$

With $\langle r^{-3}\rangle_{3d}=6.710$ a.u.$^{-3}$, $\langle 3\cos^2\theta-1\rangle_{d\pi}=2/7$, and $N^2$ taken arbitrarily as 1/2, corresponding to equal mixtures of the two atomic functions in Eq. (25), we obtain $a=0.0141$ cm$^{-1}$ and $c=0.0060$ cm$^{-1}$ to give $h_{3/2}=0.0171$ and $h_{1/2}=0.0111$ cm$^{-1}$, respectively. This value of $h_{3/2}$ is fairly close to the experimental value, but the agreement for $h_{1/2}$ is poorer.

It seems likely that the 13 343 cm$^{-1}$ and 13 079 cm$^{-1}$ levels are indeed the $v=0$ spin–orbit components of the $^2\Pi_i$ state coming from configuration (A). Consistent with this is the negative sign of the spin–rotation parameter of the ground state which, in the unique perturber approximation, indicates that there is a low-lying inverted $^2\Pi$ state. However, interactions with the nearby $^2\Sigma^+$ excited state at 13 950 cm$^{-1}$ appear to be affecting the $^2\Pi_{1/2}$ component severely. Specifically, such interaction should lower the $B$ value as observed.

As for the $\Omega'=3/2$ levels at 13 428 and 14 071 cm$^{-1}$, we have grouped them together because of their similar $B$ values. Their separation of 643 cm$^{-1}$ is slightly low for a vibrational frequency of a state with $B\sim0.55$ cm$^{-1}$, though not unduly so in view of the irregularities in the other nearby levels.

## VII. SUMMARY AND CONCLUSIONS

This work reports high resolution observations of electronic transitions of CoC, bringing to two the number of $3d$ metal monocarbides now characterized rotationally. The ground state $(9\sigma)^1$ $X\ ^2\Sigma^+$ has a large contact hyperfine parameter, which produces an unusually good example of Hund's case ($b_{\beta S}$) coupling. The energy level structure has been explored in detail, as have the hyperfine line strengths for transitions to $^2\Pi$ states. A very low-lying $^2\Delta_i$ state from the configuration $(1\delta)^3$ has been found. Its $^2\Delta_{5/2}$ component, which lies only 221 cm$^{-1}$ above $X\ ^2\Sigma^+$, $v=0$, is sufficiently populated in our experiments to allow high resolution fluorescence spectra to be taken. Various excited states have been

observed near 750 nm. Among these are what appears to be a heavily perturbed $^2\Pi_i$ state; its exact nature is unclear and must await detailed *ab initio* calculations.

## ACKNOWLEDGMENTS

Financial support from the Natural Sciences and Engineering Council of Canada is gratefully acknowledged. We thank Professor A. G. Adam (Fredericton) and Professor W. Weltner Jr. (Gainesville) for valuable comments and discussion.

[1] H. Neuhaus, R. Scullman, and B. Yttermo, Z. Naturforsch. **20a**, 162 (1965).
[2] R. Scullman and B. Yttermo, Ark. Fys. **33**, 231 (1966).
[3] O. Appelblad, R. F. Barrow, and R. Scullman, Proc. Phys. Soc. **91**, 261 (1967).
[4] A. Lagerqvist, H. Neuhaus, and R. Scullman, Z. Naturforsch. **20a**, 751 (1965).
[5] A. Lagerqvist and R. Scullman, Ark. Fys. **32**, 479 (1966).
[6] B. Kaving and R. Scullman, J. Mol. Spectrosc. **32**, 475 (1969).
[7] K. Jansson, R. Scullman, and B. Yttermo, Chem. Phys. Lett. **4**, 188 (1969).
[8] K. Jansson and R. Scullman, J. Mol. Spectrosc. **36**, 268 (1970).
[9] R. Scullman and B. Thelin, Phys. Scr. **3**, 19 (1971).
[10] R. Scullman and B. Thelin, Phys. Scr. **5**, 201 (1972).
[11] B. Simard, P. A. Hackett, and W. J. Balfour, Chem. Phys. Lett. **230**, 103 (1994).
[12] T. C. Steimle, K. Y. Jung, and B.-Z. Li, J. Chem. Phys. **102**, 5937 (1995).
[13] W. J. Balfour, J. Cao, C. V. V. Prasad, and C. X. W. Qian, J. Chem. Phys. (in press).
[14] M. D. Morse (private communication, 1994).
[15] J. M. Brom Jr., W. R. M. Graham, and W. Weltner, Jr., J. Chem. Phys. **57**, 4116 (1972).
[16] R. J. Van Zee, J. J. Bianchi, and W. Weltner, Jr., Chem. Phys. Lett. **127**, 314 (1986).
[17] Y. M. Hamrick and W. Weltner, Jr., J. Chem. Phys. **94**, 3371 (1991).
[18] B. Pinchemel and J. Schamps, Can. J. Phys. **53**, 431 (1975).
[19] R. M. Gordon and A. J. Merer, Can. J. Chem. **58**, 642 (1980).
[20] A. G. Adam, Y. Azuma, H. Li, A. J. Merer, and T. Chandrakumar, Chem. Phys. **152**, 391 (1991).
[21] W. Weltner, Jr. (private communication, 1995).
[22] A. G. Adam (private communication, 1994).
[23] B. Simard, C. Masoni, and P. A. Hackett, J. Mol. Spectrosc. **136**, 44 (1989).
[24] B. A. Palmer, R. A. Keller, and R. Engleman, Jr., Los Alamos Scientific Laboratory Unpublished Report No. LA-8251-MS, 1980.
[25] A. G. Adam, A. J. Merer, D. M. Steunenberg, M. C. L. Gerry, and I. Ozier, Rev. Sci. Instrum. **60**, 1003 (1989).
[26] C. H. Townes and A. L. Schawlow, *Microwave Spectroscopy* (Dover, New York, 1975).
[27] T. M. Dunn, in *Molecular Spectroscopy: Modern Research*, edited by K. N. Rao and C. W. Mathews (Academic, New York, 1972).
[28] R. Bacis, A. Bernard, and J. d'Incan, CR Acad. Sci. Ser. B. **273**, 272 (1971).
[29] R. Bacis and A. Bernard, Can. J. Phys. **51**, 648 (1973).
[30] R. Stringat, C. Athénour, and J.-L. Féménias, Can. J. Phys. **50**, 395 (1972).
[31] G. Herzberg, *Spectra of Diatomic Molecules*, 2nd ed. (Van Nostrand, Princeton, 1950).
[32] R. S. Mulliken, Rev. Mod. Phys. **3**, 89 (1931).
[33] A. M. James, P. Kowalczyk, and B. Simard, J. Mol. Spectrosc. **164**, 260 (1994).
[34] O. Launila and B. Simard, J. Mol. Spectrosc. **154**, 93 (1992).
[35] R. A. Frosch and H. M. Foley, Phys. Rev. **88**, 1337 (1952).
[36] A. Carrington, P. N. Dyer, and D. H. Levy, J. Chem. Phys. **47**, 1756 (1967).
[37] J. M. Brown, I. Kopp, C. Malmberg, and B. Rydh, Phys Scr. **17**, 55 (1978).
[38] A. G. Adam, Y. Azuma, J. A. Barry, A. J. Merer, U. Sassenberg, J. O. Schröder, G. Cheval, and J.-L. Féménias, J. Chem. Phys. **100**, 6240 (1994).
[39] J.-L. Féménias, C. Athénour, and R. Stringat, Can. J. Phys. **52**, 361 (1974).
[40] A. J. Merer, U. Sassenberg, J.-L. Féménias, and G. Cheval, J. Chem. Phys. **86**, 1219 (1987).
[41] M. Barnes, M. M. Fraser, P. G. Hajigeorgiou, A. J. Merer, and S. D. Rosner, J. Mol. Spectrosc. **170**, 449 (1995).
[42] W. Weltner, Jr., *Magnetic Atoms and Molecules* (Dover, New York, 1989).
[43] G. H. Guthöhrlein and H. P. Keller, Z. Phys. D **17**, 181 (1990).
[44] J. R. Morton and K. F. Preston, J. Magn. Reson. **30**, 577 (1978).
[45] T. D. Varberg, R. W. Field, and A. J. Merer, J. Chem. Phys. **95**, 1563 (1991).
[46] H. Lefebvre-Brion and R. W. Field, *Perturbations in the Spectra of Diatomic Molecules* (Academic, Orlando, 1986).
[47] T. D. Varberg, E. J. Hill, and R. W. Field, J. Mol. Spectrosc. **138**, 630 (1989).
[48] D. J. Clouthier, G. Huang, A. J. Merer, and E. J. Friedman-Hill, J. Chem. Phys. **99**, 6336 (1993).